Spray Mechanism of Contained-Electrospray Ionization

Colbert F. Miller[†], Benjamin J. Burris[†] and Abraham K. Badu-Tawiah*

Department of Chemistry and Biochemistry, The Ohio State University, Columbus, OH 43210, USA

†Authors contributed equally

*Correspondence to Dr. Abraham Badu-Tawiah 100 W. 18th Avenue, Columbus OH, 43210

Email: badu-tawiah.1@osu.edu

Tel.: 614-292-4276

Fax: (614) 292-1685

ABSTRACT

Analytical characteristics of contained electrospray ionization (ESI) are summarized in terms of its potential to modify analyte solution during the stages of droplet formation to provide opportunities to generate native versus denatured biomolecular gas-phase ions, without the need for bulk-phase analyte modifications. The real-time modification of the charged microdroplets occurs in a cavity that is included in the outlet of the contained-ESI ion source. Close examination of the inside of the cavity using high-speed camera revealed the formation of discrete droplets as well as thin liquid films in the droplets wake. When operated at 20 psi N₂ pressure, the droplets were observed to move at an average speed of 8 mm/s providing ~1 s mixing time in a 10 mm cavity length. Evidence is provided for the presence of highly reactive charged droplets based on myoglobin charge state distribution, apo-myoglobin contents, and ion mobility drift time profiles under different spray conditions. Mechanistic insights for the capture of vapor-phase reagents and droplet dynamics as influenced by different operational modes are also described.

KEYWORDS: mass spectrometry; electrospray ionization; analytical methods; accelerated droplet chemistry; mechanistic insights

INTRODUCTION

Electrospray ionization (ESI)[1, 2] is a commonly used ionization method for large biomolecular analysis by mass spectrometry (MS), since it is a soft ionization method that generates intact gas-phase ions directly from solution. Finding the optimal solution conditions is critical for structure determinations of all analytes.[3, 4] For protein analysis, non-denaturing solutions (native MS) allow the intact, folded, protein or protein complex (e.g., protein-cofactor complexes) to be transferred into gas phase without significant conformational changes or loss of cofactor.[5] Preserving protein conformations in this manner can enable the overall topology of the protein to be determined and can be related to other structural biology tools (e.g., NMR and cryo-EM).[6, 7] Denaturing solutions, on the other hand, produce unfolded proteins or protein complexes that have lost quaternary structure. Denatured protein solutions typically yield highly charged species when subjected to ESI-MS analysis. Topological information may be lost for denatured proteins, but the resultant increase in protein charge state is beneficial for two reasons 1) it allows the detection of large analytes on mass spectrometers with limited m/z range and 2) high charge states facilitate ion dissociation in tandem MS (MS/MS) experiments. Perhaps the most important advantage of ESI is its ability to serve as an interface between liquid chromatography (LC) and MS for online analysis of complex mixtures. For LC-ESI-MS applications, two separate solution conditions must be considered; solvent systems that can facilitate high resolution separations and those that will favor efficient ionization via electrospray. In some situations, the optimized mobile phase for the LC system might not be suitable for the ESI process.[8, 9]

We have recently proposed a contained-ESI ion source that has potential to provide a facile solution to this conundrum. The contained-ESI apparatus enables online modification of ESI microdroplets during MS analysis.[10, 11] This is contrary to the traditional procedures that tend to modify solutions prior to analysis.[12–15] We have shown that by using headspace vapors of acids to modify charged microdroplets derived from aqueous (native) protein solutions, the contained-ESI source was able to change the distribution of charge states of the protein in real-time.[11] The extent of change in protein charge state was found to be dependent on the pKa and vapor pressure (VP) of the acid used. The pH of the droplets can be changed in real-time simply by changing nebulizing gas pressure. With acid vapors, the process of protein unfolding is the predominant reaction, although improved signal-to-noise ratios can be achieved. The contained-ESI apparatus can also perform the reverse reaction by re-folding protein in real-time via the exposure of charged microdroplet containing previously denatured proteins to ammonium acetate/triethylammonium acetate solution.[11] Clearly, modification of solution conditions during the stages of the droplet formation can serve to provide a more flexible and efficient way to control mass spectra for biomolecules; especially when considering the ability to achieve modification on a short timescale,

suggesting compatibility with LC-MS systems, for high throughput analyses. The objective of the current study is to investigate the spray mechanism of the contained-ESI ion source to more fully understand droplet dynamics and ion structure. Such studies are important since they will allow effective optimization of this new electrospray-based ion source.

The modification of droplets in the contained-ESI source takes advantage of recent reports that show accelerated mixing, and consequently reaction rates, under the charged microdroplets environment.[16-20] Theta capillaries allow mixing times that are 2 orders of magnitude less than in any mixer previously coupled to a mass spectrometer, enabling folding and refolding of proteins to be studied on milliseconds time scale. [21–23] Enhanced bimolecular reaction rates have also been observed in charged microdroplets [24-26] and in extractive droplet fusion experiments.[27-29] The increased reaction rates are attributed to concentration and surface effects as well as effective mixing. It turns out that the difference between reactive and non-reactive electrosprayed microdroplets is derived mainly from the distance the droplets are allowed to traverse.[16, 30] Electrosprayed microdroplets become reactive at long spray distances where solvent evaporation yields droplets with high surface area-to-volume ratio. The distinguishing feature of the contained-ESI platform from other droplet-based ion sources is that it allows the generation of reactive charged microdroplets at analytical spray distances, without a substantial gap between the ion source and the inlet of the mass spectrometer. [10, 11] In fact, the contained-ESI source employs a cavity with adjustable length (1 - 10 mm) to promote droplet desolvation and to increase residence time of the droplet at larger cavity sizes, enabling effective in-situ droplet modification with reactive gases and liquids. To better understand and characterize the processes taking place within the cavity, we used a camera to examine spray dynamics. These visuals revealed the co-existence of droplets and thin liquid films within the cavity, which serve as a foundation for the reactivity of the system. Further, MS experiments were performed on myoglobin in the presence of HCl vapor, which demonstrated a charge state distribution consistent with denatured proteins. As the nebulizer gas pressure was changed, the presence of apo-myglobin versus holo-myglobin was altered, signifying that droplet pH was changed by changing the N₂ gas pressure. Droplet reactivity, indicated by higher average charge state and more apomyoglobin content, increased with increasing cavity length, which can be explained by increased reaction time in the cavity. Ion mobility spectrometry experiments confirmed MS data and corroborated the fact that by using faster droplet modification time, it is possible to generate unfolded holo-myoglobin proteins in the gas-phase that can facilitate top-down proteomics by enabling accurate molecular weight determinations prior to collisional activation of the highly charged protein ions.

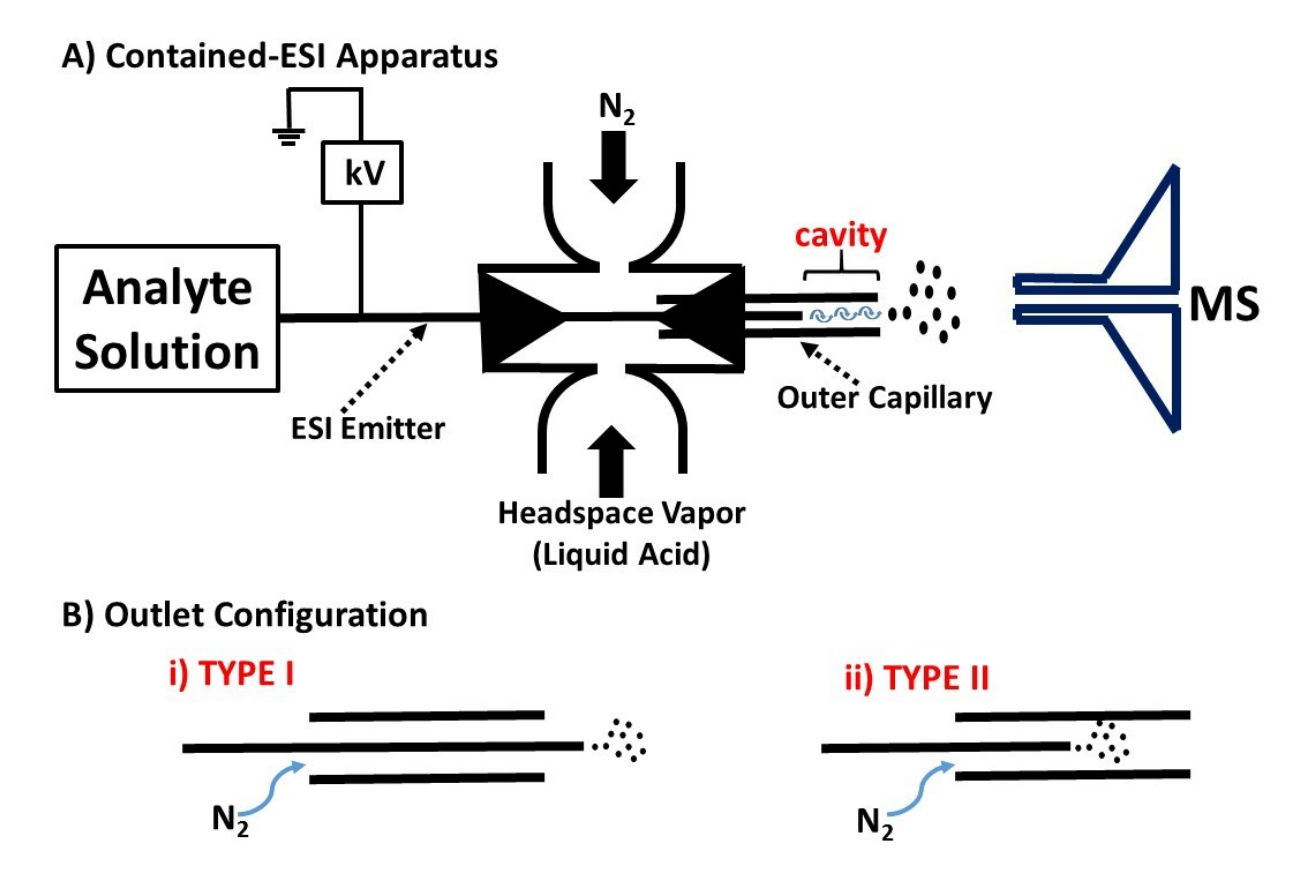


Figure 1. (A) Experimental setup for the contained electrospray ionization (ESI) platform. The apparatus uses three inputs variables (analyte solution, nebulizer gas, modifying headspace vapor), which converge in the cavity to modify charge droplets and thin liquid films prior to transport of the modified analyte to mass spectrometer. Analyte residence time is variable based on the configuration of the outlet (B): a shorter mixing time is accomplished in Type I operation mode (B,i), in which the ESI emitter is pushed out (~1 mm) of the outer capillary. In Type II mode of operation (B,ii), however, the ESI emitter is regressed creating a cavity into which the electrospray droplets form the analyte solution can be collected and modified at an extended time period (>1 s at 20 psi N₂ pressure for 10 mm cavity length).

EXPERIMENTAL SECTION

Contained-electrospray apparatus. The contained-ESI ion source (Figure 1A) has been previously described.[10, 11] In brief, the contained-ESI apparatus is constructed from a stainless steel cross Swagelok element that is capable of providing the three inputs: 1) the delivery of analyte solution via the electrospray emitter on which direct current (DC) high voltage is applied, 2) a means to modify droplet pH in real-time via the use of headspace vapor of various acids differing in pKa's and vapor pressures, and 3) a nebulizer gas (e.g., N₂) to assist in reagent mixing and ionization. These three inputs converge at the outlet of the apparatus, which we can configure in two operation modes: in Type I mode of operation (Figure 1B,i), the ESI emitter (fused silica (FS); 100 μm ID) is inserted and pushed out (~1 mm) of the outer FS

capillary (250 µm ID). This configuration affords limited interactions of the acid vapor with the electrospray droplets and hence minimal analyte modification. A cavity of variable length is created in the Type II operation mode (Figure 1B,ii) by pulling the ESI capillary inside of the outer capillary. In this case, the electrosprayed droplets accumulate as thin film on the inner surface of the outer capillary, which can be modified through the seeding of acid vapor. The dynamics of the mixing process occurring in the cavity is the subject of the current studies, which are discussed later. The electrospray emitter and the outer FS capillary are held in place by 0.2 and 0.4 mm graphite ferrules, respectively, as represented by the black triangles on either side of the apparatus shown in Figure 1A.

Videos and droplet measurements. Videos of the apparatus in use were recorded by a WATEC 704r camera with a G3.8 lens connected to a Black Magic Design Intensity Shuttle. All videos were then edited using Windows Movie Maker. Film widths and distances were measured relative to the outer diameter of the outer capillary (OD, 400 μm) using Microsoft PowerPoint using the time stamps at each frame.

Mass spectrometry. When positioned in front of a mass spectrometer, as illustrated in Figure 1A, the contained-ESI apparatus becomes an effective ion source through which large proteins and small organic compounds can be analyzed. Unless otherwise stated, the contained-ESI experimental parameters for MS analyses were: solvent flow rate: 5 μmL/min; spray voltage: 5 kV; HCl volume: 0.5 mL; 5 mm reaction cavity length. Mass spectra were collected using a Thermo Fisher Scientific Velos Pro ion trap mass spectrometer (San Jose, CA). The MS parameters were: 200 °C capillary temperature; 3 microscans; 100 ms ion injection time. Spectra were recorded for at least 30 s.

Ion mobility spectrometry (IMS). IMS was performed on a Synapt G1 HDMS instrument (Waters Corp., Milford, MA, USA). Instrument parameters were tuned to maximize signal intensity for IMS while minimizing collisional activation. The source temperature was set to 120 °C, sampling cone voltage of 200 V, extractor cone voltage of 10 V, argon flow rate in the trap was set to 7 mL/min (5.2×10^{-2} mbar), and transfer collision energy at 15 V. The T-wave settings were for trap ($300 \text{ ms}^{-1}/1.0 \text{ V}$), IMS ($300 \text{ ms}^{-1}/20 \text{ V}$), transfer ($100 \text{ ms}^{-1}/10 \text{ V}$), and trap DC bias (35 V).

Chemicals and Reagents. Myoglobin and hydrochloric acid were purchased from sigma Aldrich (St. Louis, MO, USA) and used without further purification. All samples were prepared in 100% 18.2 M Ω water from a Milli-Q water purification system (Millipore, Billerica, MA, USA).

RESULTS AND DISCUSSION

For contained-ESI MS analyses, solutions of myoglobin (MW 17.6 kDa; pI 7.4) were all prepared in 100% water. When this aqueous solution is electrosprayed in the absence of acid, myoglobin is observed in a folded, holo form which contains a non-covalently bound heme group.[11, 31, 32] Holo-myglobin is observed to undergo rapid denaturation (within 100 ms time-scale) when exposed to acid; it unfolds through a globular conformation, with the heme group still bound, before reaching the final unfolded, elongated apo form at which point the non-covalently bound heme group is lost. We chose this protein system to investigate the spray mechanism of the contained-ESI ion source because the unfolding event leading to conformational changes can be readily witnessed through changes in protein charge state distribution (CSD) during ESI-MS. The concomitant reduction in mass (due to the loss of the heme group) allows direct access to percent apo-myoglobin (% aMb), which can be used to determine the extent of myoglobin denaturation without the use of sophisticated instrumentation. The intensity-weighted average charge state (q_{avg}; equation 1)[33] was used to represent protein CSD when comparing the extent of unfolding caused by different spray conditions.

$$q_{avg} = \frac{\sum_{i=1}^{N} q_i w_i}{\sum_{i=1}^{N} w_i}$$
 Eqn 1

Where N is the number of detected charge states, q_i is the charge of the i^{th} charge state and w_i is the intensity of the i^{th} charge state.

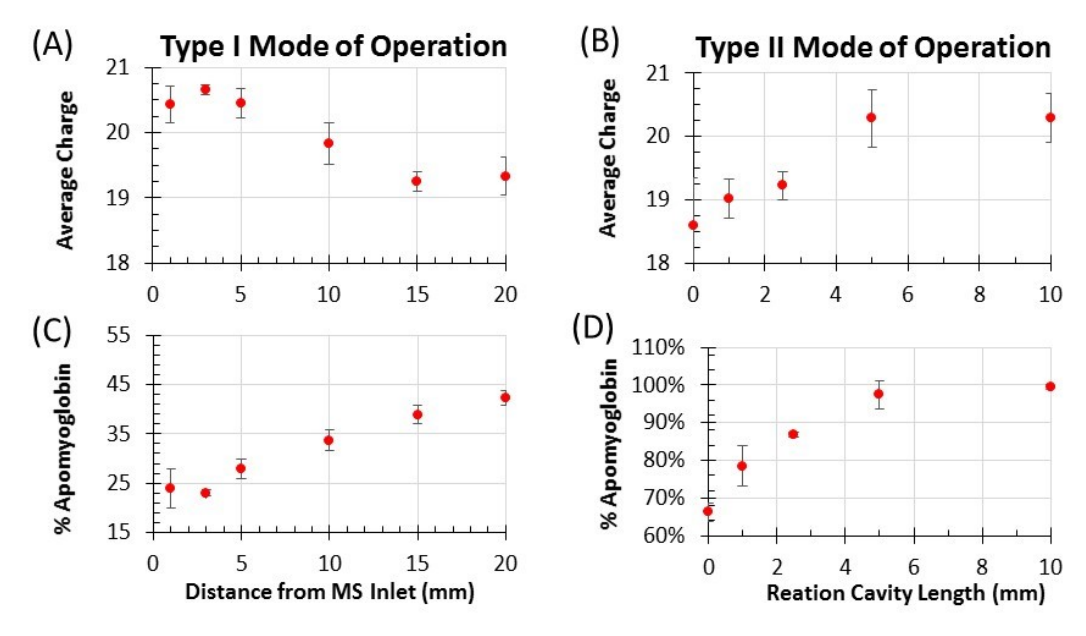


Figure 2. Comparison of reactivity between evaporating charged droplets created in Type I mode of operation (A and C) and the effect of cavity on droplet reactivity in Type II mode (B and D). The evaporating droplets were created by allowing the electrospray droplets to traverse a maximum of 20 mm distance in ambient air. Droplet reactivity was altered in Type II mode of operation by changing the cavity length from 0-10 mm. Extend of droplet reactivity was monitored both by the average charge (q_{avg}) of myoglobin (A and B) and percent apo content (C and D). Myoglobin solution (50 μ M in 100 % water) was sprayed at a flowrate of 5 μ L/min with 5 kV applied to the ESI emitter. Headspace vapor of HCl was used to modify the electrosprayed droplets in all cases.

Comparing Effects of Cavity and Droplets Evaporation on CSD and %aMb

Charged microdroplets, produced from electrospray, are routinely used to achieve accelerated bimolecular reactions.[16, 34] The assumption is that by increasing the distance between the ESI emitter and the MS inlet, the time available for desolvation of the charged microdroplets is increased, which will lead to increased concentration and surface effects. We examined this effect on protein unfolding using Type I operation mode of the contained-ESI source using different spray distances (1 – 20 mm). The Type I configuration, characterized by the absence of the cavity, is similar to conventional ESI except that the acid is not added to the protein solution; instead, the rapidly moving aqueous droplets containing the holomyoglobin were briefly exposed to HCl vapor, and the acidified droplets were allowed to travel a specified distance in ambient air. The results for this experiment are summarized in Figures 2A and C, in terms of average charge (q_{avg}) and % apo-myoglobin, respectively, for each spray distance tested. As spray distance is increased, q_{avg} showed a slight decrease in a fairly narrow range, $\Delta q_{avg} = 1.3$. We attribute the small decrease in q_{avg} to a re-folding [35–37] event as the protein is transferred in the charged microdroplet across the 20 mm distance. Although the milliseconds droplet lifetime (assuming 80 – 100 m/s droplet velocity)[27, 38] permits a small degree of myoglobin refolding, the incorporation of heme into either the

folded or unfolded protein is disfavored as this reaction requires much longer times.[31, 35] As a consequence, an increased apo content (%aMb) is observed (Figure 1C). %aMb at 20 mm spray distance was 42% indicating the majority of the protein ions were detected in the holo form. The fact that +26 charge state holo-myoglobin ions can be observed, coupled to previous works with supercharging native proteins, [11, 39] indicate that CSD alone cannot be used to effectively indicate the conformations of gas-phase protein ions. Assuming charge residue model, droplet pH can be expected to decrease as solvent evaporates,[40, 41] which should in turn facilitate protein unfolding. However, the equilibrium constant between folded and unfolded conformations of myoglobin has been reported to be stable in a wide pH range,[35] explaining why only a modest change in average charge is detected for these evaporating droplets. Collectively, these results suggest that rapidly moving charged microdroplets can be modified, but concentrations and pH effects due to solvent evaporation afford a limited droplet reactivity reducing the extend of protein denaturation.

Instead of utilizing long spray distances, which can present the unwanted consequence of inefficient ion transport to the distant mass spectrometer, we proposed to extend mixing time of droplets with vapors by introducing an enclosed space before the droplets are transported to the MS. Within this cavity, analytes are sprayed from the electrospray emitter and are transported along the length of the outer FS capillary, during which time the droplets and films can interact with the headspace vapor (Type II operation mode). The volume of the cavity was controlled by changing its length (0 - 10 mm; i.e., distance between ESIemitter tip and the tip of the outer capillary). The N_2 nebulizing gas induces mixing of reagents and carries the acidified analyte solution to the MS in the form of modified charged droplets. We kept the distance from the tip of the outer capillary to the MS inlet constant (2 mm) for all experiments. To compare reactivity in the cavity with that derived from the evaporating droplets, we monitored q_{avg} and %aMb. The average charge state showed a gradual increase with increasing cavity length (Figure 2B), but like the evaporating droplets derived from the Type I operation mode, the difference was fairly small ($\Delta q_{avg} = 1.7$). Assuming constant charge, turbulent mixing can be more effective at longer cavity lengths and lead to a more profound impact of the acid on the pH of the droplet. Also, reaction time is expected to increase at longer cavity lengths (discussed later); plus, the turbulent flow itself characterized by chaotic pressure changes can further cause protein unfolding. In fact, based on measure droplet velocity (6 mm/s at 50 psi) in the cavity and estimated kinematic viscosity coefficient (v) of 8.9×10^{-7} m²/s for water, we calculated Reynold's number (Re = uL/v (u = velocity in the fluid flow, L = is spatial scale, e.g., length) to be ~90, confirming the existence of turbulence flow in the microliter size cavity of length 10 mm. pH effects and turbulent gas flow can explain the observed increase in q_{avg} for the Type II operation mode. Evidence for extended protein unfolding can be found not only in the increased average charge state, but also in the increased %aMb (Figure 2D). Even at zero cavity length (i.e., the ESI emitter is neither pushed out nor pulled inside of the

outer capillary; rather the two capillaries are at equal lengths at the outlet of the contained-ESI source), we detected 66% apo content, which is >20% more than the effect observed for evaporating droplets at 20 mm spray distance. This signifies a change in spray dynamics that can result from two distinct effects: 1) since the outer capillary is at equidistant with the electrospray inner capillary, the capture of HCl vapor can begin in the Taylor cone, where mixing is known to be efficient as in the case for theta capillaries, and/or 2) increase shear force of the nebulizer gas on analyte solution. At zero-length cavity,[42] the N₂ gas and the analyte solution exit the contained-ES source at the same point in space, compared with Type I mode where the solution is ahead of the gas and therefore interacts with the gas in a diffused region. Apo-myoglobin content reach 97% when cavity length was increased to 5 mm. These results confirm that the presence of cavity in the contained-ESI ion source allows for the creation of more reactive electrospray environment for effective modification of analyte solution in real-time while still using analytical spray distance of 2 mm.

Effects of Sheath Gas in Contained-Electrospray Ionization

The nitrogen nebulizer gas exerts four interrelated effects in the contained-ESI ion source: (1) variable droplet speed at different N2 pressures (which in turn controls the extent to which the analyte interacts with the modifying HCl vapor), (2) controls vapor pressure of HCl that is sampled, through suppression and/or dilution effects, (3) facilitates mixing via turbulent flow in the cavity, and (4) finally, the level of ion yield. As already discussed, the Type I operation mode offered limited effect because of the limited amount of time the droplets have to interact with the reagent vapor. Previous experiments showed that the droplet pH is ~1.2 at 30 psi N₂ pressures, which increased to pH of 4.5 upon increasing N₂ pressure to 140 psi. These results were corroborated by measured HCl consumption rates of 6.4 nL/min and 3.3 nL/min for 30 and 140 psi N₂ pressures, respectively. The concentration of HCl headspace vapor decreased with increasing pressure, which was accompanied by a concomitant increase in droplet speed. Stills from movies recorded for the Type I operation mode at 20 and 100 psi nebulizer pressures are provided in Figure S1, which show visible droplets and bulky Taylor cone when the spray occurs using 20 psi. The Taylor cone is seen originating from the outer capillary, which is 1 mm behind the ESI emitter from which the protein solution is delivered. Since the HCl vapor is carried by the N₂ gas and is delivered through the outer capillary, the presence of a large stable Taylor cone at 20 psi can translate into more efficient vapor capture into the analyte solution. On the contrary, the droplets produced when using 100 psi N₂ pressure in the Type I mode were too small and fast to be observed by WATEC 704r camera used here (Figure S1C). At such high nebulizing gas pressure, a very small Taylor cone is observed localized only on the ESI capillary suggesting limited droplet exposure to HCl vapor. These insights revealed by the imaging experiments are

consistent with measured droplet pH, reagent consumption rates and previously reported droplet reactivity.[10, 11]

Unlike the Type I operation mode, which can produce fairly good ion yields independently of spray voltage and nebulization, the Type II mode of the contained-ESI source embodying the reaction cavity requires simultaneous application of DC voltage and nebulizer gas (Figure 3). In the absence of applied voltage the analyte solution delivered into the cavity can be nebulized and pushed along via turbulent flow but the solution accumulates in a big drop upon arriving at the tip of the outer capillary (Figure 3B). This is due to the lack of electric field gradient required for Taylor cone formation. With the ESI emitter regressed into the outer capillary, enough momentum garnered from pneumatic effects derived from the pressurized device is necessary to allow effective transport of droplets/ions to the mass spectrometer. Also, in the absence of applied N₂ gas, there is neither thin film nor droplet formation in the cavity, which results in a significantly reduced ion yield (Figures 3A and C).

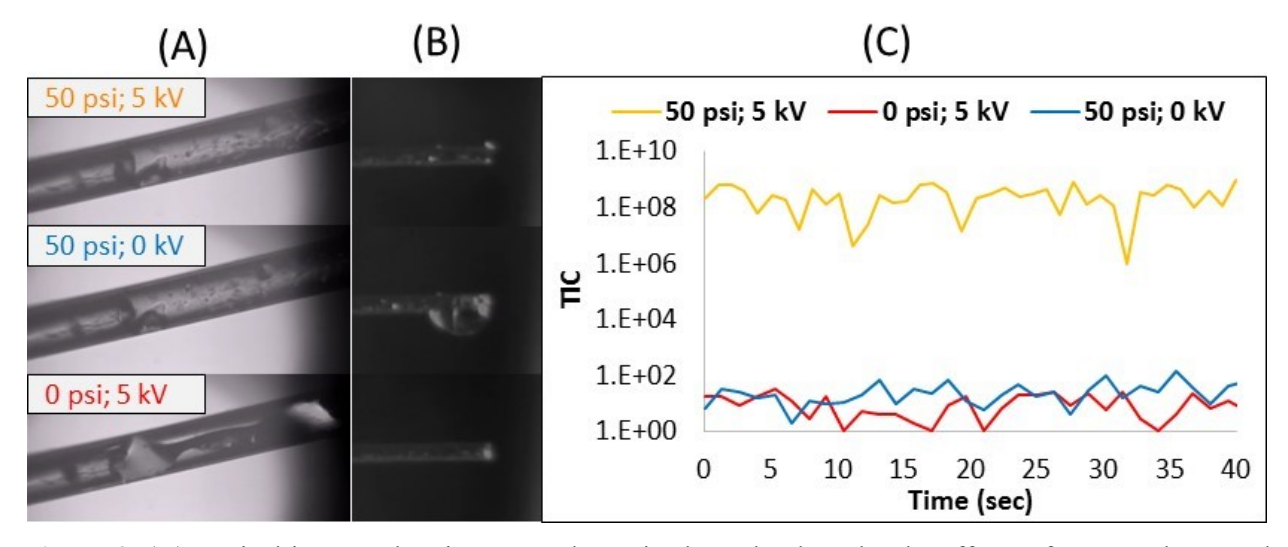


Figure 3. (A) Optical images showing spray dynamics brought about by the effects of spray voltage and nebulizer gas pressure in relation to the position of the ESI-emitter in the reaction cavity in Type II mode. (B) Close-up images of the outlet of the cavity indicating that the absence of electric field (0 kV) leads to the accumulation of analyte solution into a big drop. (C) Total ion chronogram (TIC) showing the effect of spray voltage and N_2 nebulizer gas pressure on the intensity of ion current.

Mass spectra for myoglobin recorded at different N₂ pressures when the contained-ESI source was operated in Type II mode are shown in Figure 4A. The different CSDs observed here can serve to indicate pH changes in the cavity as the nebulizing gas pressure is changed. We expect longest HCl vapor exposure times in the cavity at low N₂ pressures and hence a more complete protein denaturation. As anticipated, all holo-myoglobin proteins originally present in aqueous solution were converted into apo form (100% aMb) when using 20 psi N₂ gas pressure (Figure 4A,i). Apo-myoglobin content decreased to 81% upon increasing the pressure from 20 to 50 psi, although q_{avg} remained similar (Figure 4A,ii). Apo-myoglobin content further

decreased to 68% at 100 psi, with a concomitant decrease in q_{avg} from 22 to 14 (Figure 4A,iii). These results are attributed to the combined effects of changes in pH and exposure times in the cavity. The presence of slow moving droplets combined relatively bulky liquid thin films at 20 psi N₂ pressure means that the capture of HCl vapor will be more efficient causing significant drop in pH (<1.2 pH units) [10], which explains why holo-myoglobin species did not survive this spray condition. In Type I mode of operation, the bigger size of the Taylor cone created at lower N₂ gas pressure exerts similar effects by facilitating absorption of HCl vapor into the droplets. Closer examination of peaks derived from apo-myoglobin (e.g., see +15 charge state, Figure 4B) revealed high HCl adduction at lower pressures – 8 and 4 HCl adducts were detected for 20 and 50 psi, respectively. Although pKa (-7) of HCl should facilitate its complete dissociation in the cavity, the detection of HCl adducts is not surprising if we consider the time scale of the mixing process, which has been shown experimentally to be on seconds timescale (discussed later). Number of HCl adduction decreased with increasing pressure because of the overall decrease in the concentration of HCl headspace vapor. No HCl adducts were observed at 100 psi N₂ pressure. Instead, sodium adducts emerged indicating higher pH in the cavity relative to the lower pressures tested. It is important to note that these experiments occurred with low source currents, which minimized possible oxidation reactions during the electrospray process. In contrast, low signal-to-noise ratios and high source currents were detected when HCl was directly added to myoglobin solution (pH 1.3) and analyzed by conventional ESI-MS (Figure S2). Unlike the contained-electrospray source which showed clear and resolved HCl adducts after exposure of droplets to HCl vapor, electrospray of the acidified myoglobin solution produced a broad peak extending over 20 m/z range. This is possibly caused by the high conductivity of the initial protein solution in the presence of HCl, which can lead to protein oxidation. In this regard, it is clearly advantageous to modify droplets instead of analyte solution.

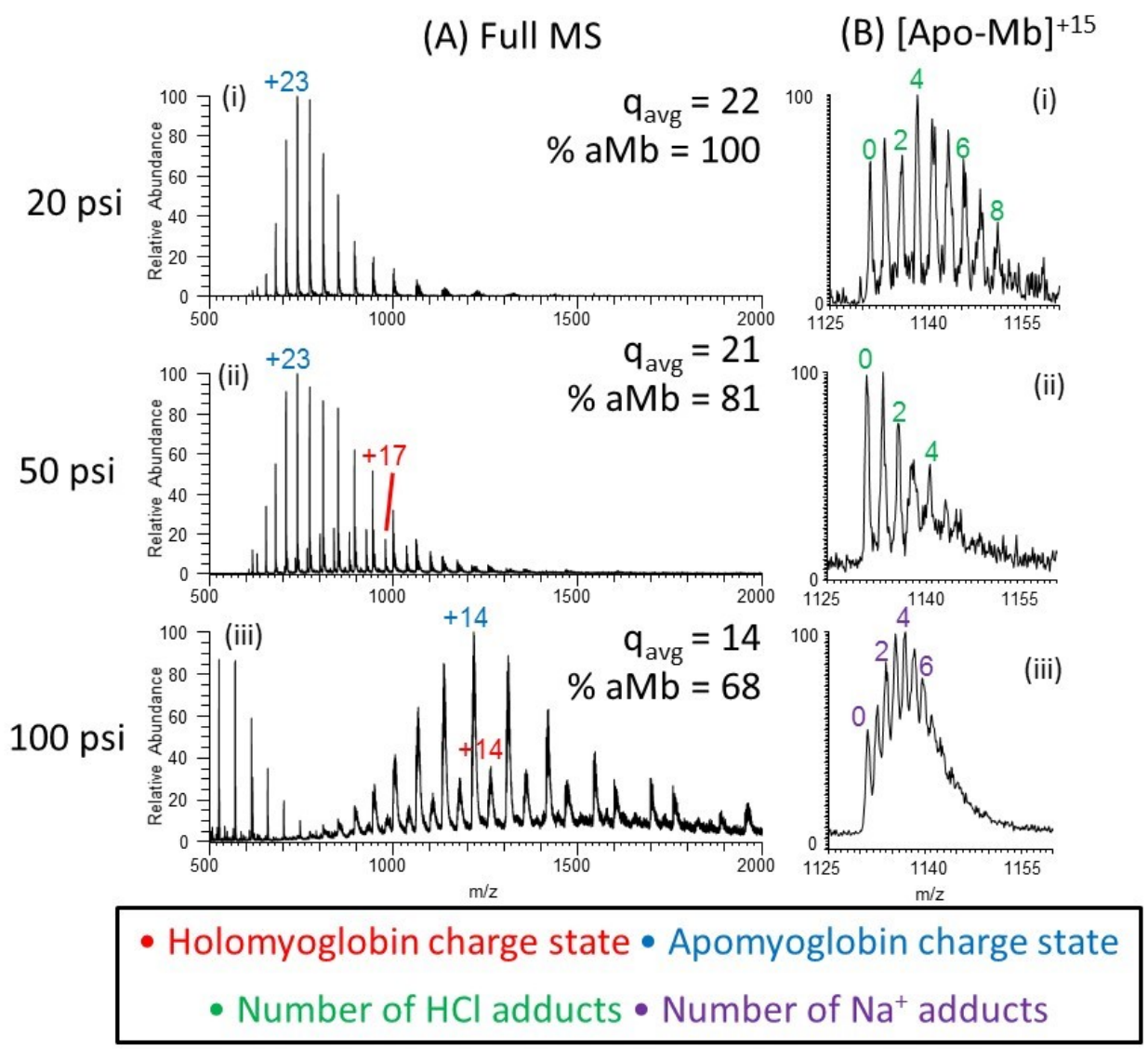


Figure 4. (A) Positive-ion mode contained-ESI mass spectra showing myoglobin ion distribution at 20 psi (A,i), 50 psi (A,ii) and 100 psi (A,iii) N_2 gas pressures. (B) Zoomed-in spectra for +15 apo-myoglobin charge state showing varied number of adducts: <8 HCl (B,i), <4 (B,ii) and <6 Na^+ (B,iii) attachments as a function of N_2 pressure at 20, 50, and 100 psi, respectively.

Mechanistic Insights and Spray Dynamics in the Reaction Cavity of the Contained-ESI Source

Videos of Type II spray mode showed the presence of droplets and thin liquid films in the cavity (Videos S1-6). The analyte solution from the ESI emitter is initially sprayed along the walls of the outer capillary, inside the cavity, as thin liquid films. The vigorous turbulence mixing caused by N_2 carrier gas leads to instantaneous breakup of the thin liquid film. The fast gas flow also carry solvent vapor away from the surface of the droplets, thereby promoting evaporation. The process is balanced by the continuous feed of analyte solution into the cavity, compensated by the evaporative loss. This steady state culminates in the

formation discontinuous thin liquid film within which tiny droplets are dispersed. Depending of angle and level of illumination these two microreactors can be visualized individually and their speed and sized measured. Videos S1-3 show the formation of discrete droplets in the cavity, while Videos S4-6, obtained by using a brighter back light and closer camera, show liquid films present in the droplets wake. Solution that reaches the end of the cavity forms larger drops at the tip of the outer capillary, which produces progeny droplets in the presence of applied electric field. Apparently, the discontinuous nature of the spray and the strong desolvation occurring in the cavity allows charge build-up, which enables the formation Taylor cone from droplets in the reaction cavity before reaching the tip of the outer capillary (Video S7). At low solvent flowrates ($<3~\mu$ L/min), the strong turbulent flow in the cavity is enough to unfold myoglobin (80% apo content) even in the absence HCl vapor.[11]

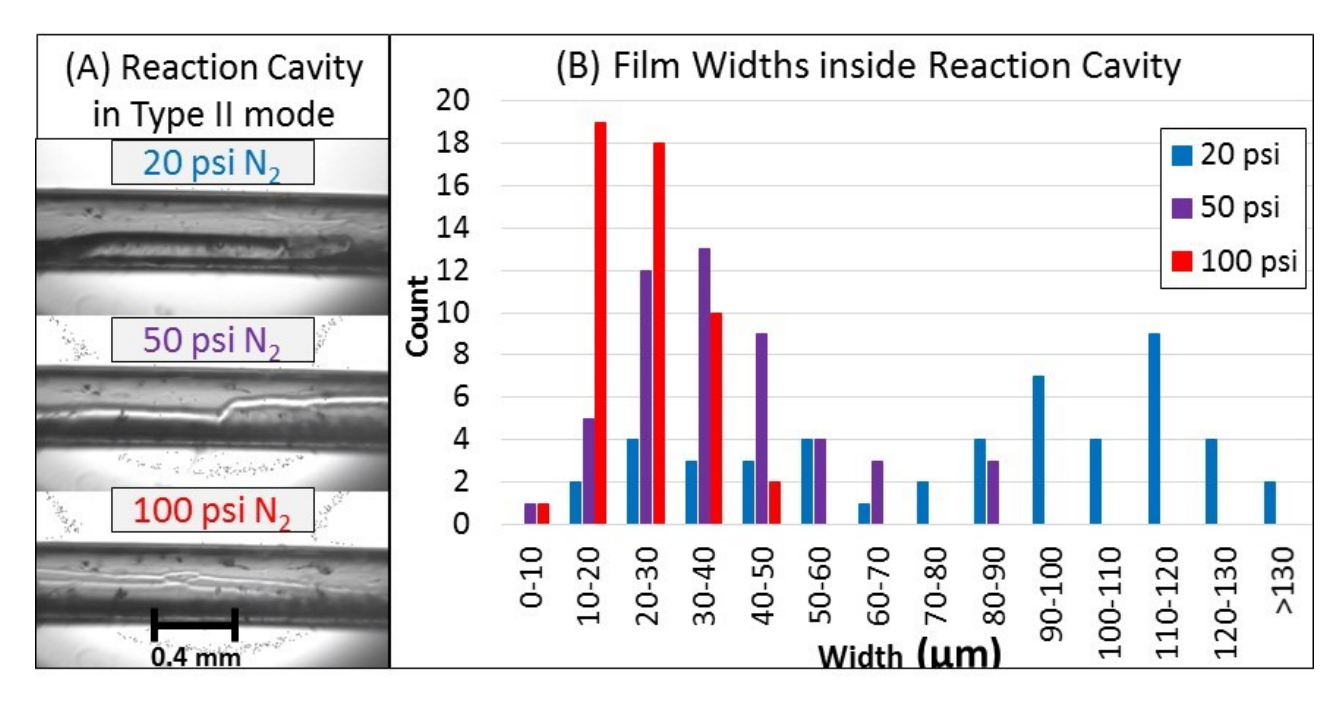


Figure 5. The effects of N₂ gas pressures on film size during Type II mode operation. (A) Optical images showing typical liquid thin films observed using brighter back light and closer camera at 20, 50 and 100 psi nebulizing pressures. (B) Histogram summarizing the distribution of film widths at 20, 50 and 100 psi nebulizing pressures. Higher nebulizer pressures produced smaller and a more narrow distribution in film thickness confirming rapid solvent evaporation in the cavity.

Table 1. Summary of droplet velocities inside the reaction cavity during Type II operation mode at different nebulizer gas pressures[#]

N ₂ Pressure (psi)	Average Droplet Velocity ± std. dev. (mm/s)	High Velocity (mm/s)	Low Velocity (mm/s)
20	7.6 ± 5.6	16	0.4
50	6.3 ± 4.8	16	2.2
100	11 ± 14	40	2.0

^{*}Droplet velocities were measured in directions toward the outer of the cavity. Average velocity was calculated from many droplets in cavity, each receiving two to six separate measurements.

Owing to our ability to preferentially image droplets over liquid film (and vice versa) in the cavity, we were able to further characterize size and speed of these two microreactors in an actual spray process. The results of these experiments are summarized in Table 1 for droplets, and Figure 5 for thin liquid films at three different N2 nebulizer pressures (20, 50 and 100 psi). The associated mass spectra at each nebulization pressure are provided in Figure 4 above. In general, droplet velocity in the cavity, measured along the direction of the outer capillary toward the outlet, increased with N_2 pressure. The highest velocity recorded was 40 mm/s for 100 psi N₂ pressure and the lowest was 0.4 mm/s for 20 psi. These represent a significant reduction ($>10^3$ orders of magnitude) in droplet speed when compared with the velocity (~ 100 m/s) of charged microdroplet derived from traditional electrospray emitter operating at 100 psi N₂ pressure. The obvious reduction in droplet speed can explain the extreme droplet reactivity observed in the cavity, exemplified by the fact that as small as 1 mm cavity length is able exert more denaturation effect (78% apo content) than evaporating droplets travelling at a speed of ~100 m/s over 20 mm spray distance (42% apo content). Data presented here suggest that on average, a droplet spends about 1 s in a 10 mm the reaction cavity. It is important to note that the chaotic nature of droplet movement in the cavity makes such measurements challenging, resulting in large variations, indicated by the standard deviations. We measured each droplet two to six times depending on the length of time we were able to observe it. An average droplet size of approximately 15 μm (diameter) was observed in the cavity at 5 kV spray voltage and 100 psi N₂ gas pressure, with a tight distribution ranging from size 10 to 50 µm (Figure S3). This distribution shifted toward large droplet size as N2 gas pressure was decreased, as would be expected for reduced desolvation in the cavity. Average droplet size of 28 µm observed at 50 psi. Bimodal droplet distribution of droplet sizes emerged upon further decrease of N₂ pressure to 20 psi, which centered at 35 and 100 μm (Figure S3).

Analyses of thin films formed in the cavity during contained-ESI also showed large variations in film widths, but the effect of nebulizer gas pressure on film width was obvious (Figure 5B). At 20 psi, thin liquid film width ranged from \geq 10 to >130 μ m (mean 85 μ m; median 93 μ m; standard deviation 37 μ m).

Bigger films (width >90 μm) were observed more frequently, signifying a weak turbulent flow at the low pressure. Upon increasing the pressure to 50 psi, while keeping the solution flow rate constant at 5 μm/min, the bigger liquid films disappeared, indicating increased desolvation rate in the cavity, which reduced average film width to 38 μm (median 35 μm; standard deviation 18 μm). Further increase of nebulizing gas pressure to 100 psi produced a narrow range of liquid films centered at an average width of 24 um (median 23 μm; standard deviation 8.5 μm). Representative images of the thin films at the three pressures tested are shown in Figure 5A. The histogram analyses provided in Figure 5B were based on the measurement of 50 individual films at each pressure. Collectively, the dynamics of droplets and thin films in the cavity collaborate well with protein CSD recorded in Figure 4A at different pressures. Slow moving droplets combined with relatively bulky liquid thin films at lower nebulizing pressure suggests a more efficient capture of HCl vapor and more time for reaction. At higher pressures, where the rate solvent evaporation can be expected to be higher than rate of solvent input, the capacity of the resultant thinner liquid films to dissolve the HCl vapor is reduced limiting protein unfolding reactions.

Ion Mobility Spectrometry Analysis of Ions from Different Spray Modes

Comparable average charged states were measured for Types I and II operation modes, but the species registered markedly different %aMb (Figure 2). This suggests that the extent of denaturation is not the same although charge states are comparable. To investigate whether the changes in %aMb observed here actually corresponds to protein conformational changes, we performed ion mobility spectrometry (IMS) experiments using five different spray conditions. The conventional electrospray experiment involved two myoglobin solutions prepared in pure water and in 1% acetic acid. For contained-electrospray conditions, we used Type I mode and Type II spray mode, which embodied two different cavity lengths at 5 and 10 mm. All the contained-electrospray experiments were performed in the presence of HCl vapor, without direct addition to the analyte solution. The ion mobility drift time profiles from these five experiments are provided in Figure 6 and show obvious differences in the shape and position of the peaks. At the two extremes, the electrospray analysis performed in pure water showed a relatively narrow peak centered at a drift time of 4.4 ms (violet trace) whereas the analysis conducted in the presence of 1% acetic acid yielded a broader peak located at 2.3 ms (green trace). These results are consistent with previous reports based on MS analyses which registered a narrow CSD for myoglobin solutions sprayed from pure water. [11, 32] The decreased drift time observed in the presence of acid reflects reduced apo content (from heme loss) and increased charge state both of which signify conformational changes resulting from protein denaturing.

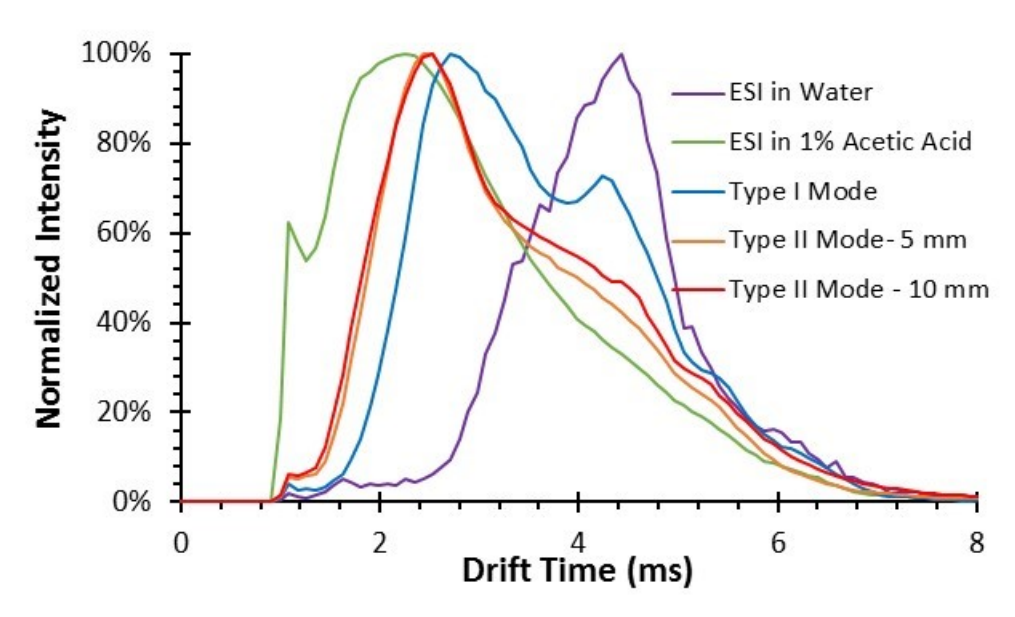


Figure 6. Comparison of ion mobility drift time profiles for five different spray conditions: conventional electrospray of myoglobin from 100% water (violet trace) and 1% acetic acid (green trace), and contained-ESI operated in Types I (blue trace) and II mode (5 mm (orange trace) and 10 mm (red trace) cavity lengths) in the presence of HCl vapor. N₂ gas pressure of 20 psi was used for all experiments.

The blue trace in Figure 6 shows the drift time profile recorded when using the contained-ESI source in Type I mode. The appearance of two obvious peaks at 2.8 and 4.2 ms indicates two possible ion conformations were produced from this spray mode, which are derived from brief exposure of the aqueous droplets to HCl vapor. As indicated in Figure 2C, the Type I spray mode is expected to yield ~28% apo content at the 5 mm spray distance used for this ion IMS experiments, so the appearance of the native-like peak at 4.2 ms is not surprising. What is surprising is the fact that though the majority of the ions are in the holo form, they were detected at shorter 2.8 ms drift time indicating some degree of protein unfolding. However, the extent of unfolding is comparably less than that observed when the protein was exposed to acetic acid in bulk solution as indicated by even shorter drift time (2.3 ms). Note: similar q_{avg} for ESI in 1% acetic acid and Type I (HCl vapor) spray mode were observed at 19.2 and 20.8, respectively; also the most abundant charge states were +21 and +22, respectively.[11] These data suggest that the difference in drift times is due mainly to differences in apo-myoglobin content, with the contained-ESI source providing a more accurate measurement due to its ability to retain the heme co-factor even at such high charge states. Such a capability will be extremely useful for the characterization of previously uncharacterized protein complexes in top-down proteomics where accurate molecular weight information will be needed before MS/MS analysis. To further investigate this possibility, we extracted the ion mobility drift time profiles for charges +19, +20, +21 and +22 for conventional ESI versus contained-ESI. In all cases, we observed a gradual decrease in drift time as charged state increased indicating modest charge/conformational effects (Figure S4). The mass effect was, however, obvious with ions (mixture of holo and apo proteins) from the

Type I spray mode compared to ions (apo only) derived from the conventional ESI source. Ion mobility drift time profiles were also recorded for ions generated from the Type II spray mode of the contained-ESI source (Figure 6); at 5 mm cavity length, we observed a small shoulder (centered at 4.2 ms; red trace), which decreased in size upon increasing cavity length to 10 mm. This data confirms MS results which revealed ~3% holo-myoglobin content when the protein was exposed to HCl vapor at the same 5 mm a cavity length (Figure 2D). Extracted ion mobility drift time profiles for the Type II spray mode did not show significant difference when compared with in-solution protein modification (Figure S4); this results is not surprising considering that charge state and apo content are comparable to that of ions generated from acidified (1% acetic acid) myoglobin solution.

CONCLUSIONS

The contained-electrospray process described here provides real-time modification of protein analytes offering effective control of the mass spectrometer output in terms of the generation of native versus denatured gas-phase ions without extensive solution-phase modification prior to mass analysis. We envision that the contained-electrospray ion source will serve as an effective interface for liquid chromatography-mass spectrometry to improve analytical sensitivity for both small and large biomolecules by providing opportunities to select suitable mobile phase without compromising electrospray ion yield. The modification of the electrospray microdroplet occurs in a cavity, which is embodied at the outlet of the contained-electrospray emitter. Movies recorded during contained-electrospray reveal the existence of both thin liquid films and droplet inside the cavity. This is important because both the droplet and the liquid thin film are well-known microreactors that can accelerate chemical reactions. Their detection in this study proves that the cavity in the contained-electrospray ionization is a unique reaction system. For example, mass spectrometry experiments showed thin liquid film/droplets generated in a 1 mm cavity to be more reactive than when the droplets are allowed to traverse a 20 mm distance in ambient air. The effect of nebulizer gas pressure on width of thin film and droplet size was characterized, which corroborated well with myoglobin charge state distribution, percent apo content, and ion mobility drift times and profiles. The observed increase in myoglobin charge state distribution and apo content with decreasing nebulizer gas pressure were ascribed to increased analyte residence time as a result of reduced droplet speed in the cavity. Reduced nebulizer gas also caused reduced pH due to effective capture of the HCl modifying reagent and hence more effective myoglobin denaturation. Both MS and ion mobility spectrometry experiments confirmed that, when operated in the absence of the cavity (Type I mode), the contained-electrospray produced highly charged holo-myoglobin species due to short droplet lifetimes. In essence, by controlling the mode of operation, correct molecular weight information about a labile protein can be obtained under

acidic conditions while also offering the opportunity to facilitate tandem MS fragmentation and protein sequencing through the formation of highly charged protein ions.

ASSOCIATED CONTENT

Supporting Information

The Supporting Information is available free of charge on the ACS Publications website.

Videos and still images of the spray, comparison of effect of acid under bulk and droplet reaction, and ion mobility data on selected charge states. (PDF)

AUTHOR INFORMATION

Corresponding Author

*E-Mail: badu-tawiah.1@osu.edu

ACKNOWLEDGEMENTS

This research was supported by the National Science Foundation (grant numbers CHE-1900271 and CHE-1801971) and the U.S. Department of Energy, Office of Science, Office of Basic Energy Sciences, Condensed Phase and Interfacial Molecular Science, under award number DE-SC0016044. The authors thank Dr. Vicki Wysocki's lab at The Ohio State University for assistance with ion mobility analysis.

REFERENCES

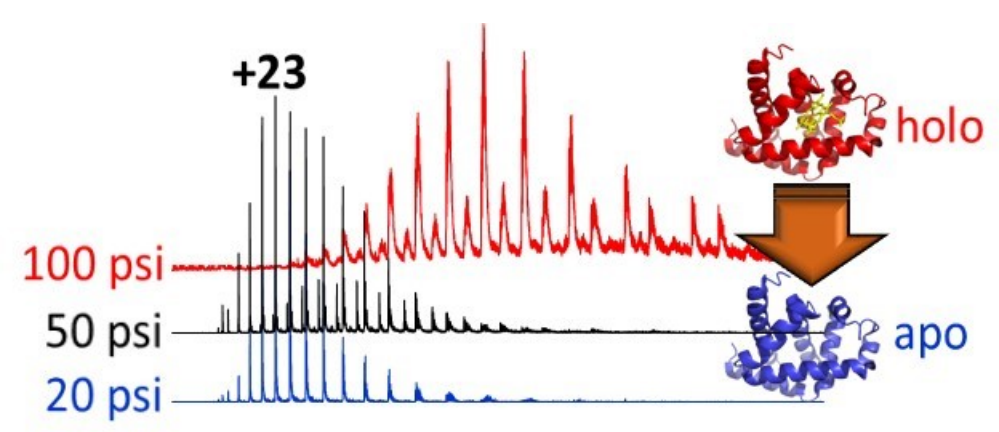
- 1. Fenn, J., Mann, M., Meng, C., Wong, S., Whitehouse, C.: Electrospray ionization for mass spectrometry of large biomolecules. Science. 246, 64–71 (1989). https://doi.org/10.1126/science.2675315
- 2. Wilm, M.: Principles of electrospray ionization. Mol. Amp Cell. Proteomics. mcp.R111.009407 (2011). https://doi.org/10.1074/mcp.R111.009407
- 3. Kostiainen', R.: Effect of Solvent on Dynamic Range and Sensitivity in Pneumatically-assisted Electrospray (Ion Spray) Mass Spectrometry. 7
- 4. Mallet, C.R., Lu, Z., Mazzeo, J.R.: A study of ion suppression effects in electrospray ionization from mobile phase additives and solid-phase extracts. Rapid Commun. Mass Spectrom. 18, 49–58 (2004). https://doi.org/10.1002/rcm.1276
- 5. Leney, A.C., Heck, A.J.R.: Native Mass Spectrometry: What is in the Name? J. Am. Soc. Mass Spectrom. 28, 5–13 (2017). https://doi.org/10.1007/s13361-016-1545-3
- 6. Urnavicius, L., Zhang, K., Diamant, A.G., Motz, C., Schlager, M.A., Yu, M., Patel, N.A., Robinson, C.V., Carter, A.P.: The structure of the dynactin complex and its interaction with dynein. Science. 347, 1441–1446 (2015). https://doi.org/10.1126/science.aaa4080
- 7. Liko, I., Allison, T.M., Hopper, J.T., Robinson, C.V.: Mass spectrometry guided structural biology. Curr. Opin. Struct. Biol. 40, 136–144 (2016). https://doi.org/10.1016/j.sbi.2016.09.008

- 8. Banks, J.F., Whitehouse, C.M.: Electrospray Ionization Mass Spectrometry. Methods Enzymol. 270, 486–519 (1996)
- 9. Garcia, M.: The effect of the mobile phase additives on sensitivity in the analysis of peptides and proteins by high-performance liquid chromatography–electrospray mass spectrometry. J. Chromatogr. B. 825, 111–123 (2005). https://doi.org/10.1016/j.jchromb.2005.03.041
- Kulyk, D.S., Miller, C.F., Badu-Tawiah, A.K.: Reactive Charged Droplets for Reduction of Matrix Effects in Electrospray Ionization Mass Spectrometry. Anal. Chem. 87, 10988– 10994 (2015). https://doi.org/10.1021/acs.analchem.5b02943
- Miller, C.F., Kulyk, D.S., Kim, J.W., Badu-Tawiah, A.K.: Re-configurable, multi-mode contained-electrospray ionization for protein folding and unfolding on the millisecond time scale. The Analyst. 142, 2152–2160 (2017). https://doi.org/10.1039/C7AN00362E
- 12. Loo, R.R.O., Dales, N., Andrews, P.C.: Surfactant effects on protein structure examined by electrospray ionization mass spectrometry. Protein Sci. 3, 1975–1983 (1994). https://doi.org/10.1002/pro.5560031109
- 13. Zhou, M., Dagan, S., Wysocki, V.H.: Protein Subunits Released by Surface Collisions of Noncovalent Complexes: Nativelike Compact Structures Revealed by Ion Mobility Mass Spectrometry. Angew. Chem. Int. Ed. 51, 4336–4339 (2012). https://doi.org/10.1002/anie.201108700
- 14. Zhuang, X., Gavriilidou, A.F.M., Zenobi, R.: Influence of Alkylammonium Acetate Buffers on Protein–Ligand Noncovalent Interactions Using Native Mass Spectrometry. J. Am. Soc. Mass Spectrom. 28, 341–346 (2017). https://doi.org/10.1007/s13361-016-1526-6
- 15. Sterling, H.J., Prell, J.S., Cassou, C.A., Williams, E.R.: Protein Conformation and Supercharging with DMSO from Aqueous Solution. J. Am. Soc. Mass Spectrom. 22, 1178–1186 (2011). https://doi.org/10.1007/s13361-011-0116-x
- 16. Yan, X., Bain, R.M., Cooks, R.G.: Organic Reactions in Microdroplets: Reaction Acceleration Revealed by Mass Spectrometry. Angew. Chem. Int. Ed. 55, 12960–12972 (2016). https://doi.org/10.1002/anie.201602270
- 17. Badu-Tawiah, A.K., Eberlin, L.S., Ouyang, Z., Cooks, R.G.: Chemical Aspects of the Extractive Methods of Ambient Ionization Mass Spectrometry. Annu. Rev. Phys. Chem. 64, 481–505 (2013). https://doi.org/10.1146/annurev-physchem-040412-110026
- 18. Banerjee, S., Gnanamani, E., Yan, X., Zare, R.N.: Can all bulk-phase reactions be accelerated in microdroplets? The Analyst. 142, 1399–1402 (2017). https://doi.org/10.1039/C6AN02225A
- 19. Mondal, S., Acharya, S., Biswas, R., Bagchi, B., Zare, R.N.: Enhancement of reaction rate in small-sized droplets: A combined analytical and simulation study. J. Chem. Phys. 148, 244704 (2018). https://doi.org/10.1063/1.5030114
- Jayaraj, S., Badu-Tawiah, A.K.: N-Substituted Auxiliaries for Aerobic Dehydrogenation of Tetrahydro-isoquinoline: A Theory-Guided Photo-Catalytic Design. Sci. Rep. 9, 11280 (2019). https://doi.org/10.1038/s41598-019-47735-y
- 21. Mortensen, D.N., Williams, E.R.: Theta-Glass Capillaries in Electrospray Ionization: Rapid Mixing and Short Droplet Lifetimes. Anal. Chem. 86, 9315–9321 (2014). https://doi.org/10.1021/ac502545r

- 22. Fisher, C.M., Kharlamova, A., McLuckey, S.A.: Affecting Protein Charge State Distributions in Nano-Electrospray Ionization via In-Spray Solution Mixing Using Theta Capillaries. Anal. Chem. 86, 4581–4588 (2014). https://doi.org/10.1021/ac500721r
- 23. Radionova, A., Greenwood, D.R., Willmott, G.R., Derrick, P.J.: Dual Nano-Electrospray and Mixing in the Taylor Cone. Mass Spectrom. Lett. 7, 21–25 (2016). https://doi.org/10.5478/MSL.2016.7.1.21
- 24. Banerjee, S., Zare, R.N.: Syntheses of Isoquinoline and Substituted Quinolines in Charged Microdroplets. Angew. Chem. 127, 15008–15012 (2015). https://doi.org/10.1002/ange.201507805
- 25. Müller, T., Badu-Tawiah, A., Cooks, R.G.: Accelerated Carbon⊡Carbon Bond-Forming Reactions in Preparative Electrospray. Angew. Chem. Int. Ed. 51, 11832–11835 (2012). https://doi.org/10.1002/anie.201206632
- 26. Marsh, B.M., Iyer, K., Cooks, R.G.: Reaction Acceleration in Electrospray Droplets: Size, Distance, and Surfactant Effects. J. Am. Soc. Mass Spectrom. 30, 2022–2030 (2019). https://doi.org/10.1007/s13361-019-02264-w
- 27. Lee, J.K., Kim, S., Nam, H.G., Zare, R.N.: Microdroplet fusion mass spectrometry for fast reaction kinetics. Proc. Natl. Acad. Sci. 112, 3898–3903 (2015). https://doi.org/10.1073/pnas.1503689112
- 28. Chen, H., Venter, A., Cooks, R.G.: Extractive electrospray ionization for direct analysis of undiluted urine, milk and other complex mixtures without sample preparation. Chem. Commun. 2042 (2006). https://doi.org/10.1039/b602614a
- 29. Marquez, C.A., Wang, H., Fabbretti, F., Metzger, J.O.: Electron-Transfer-Catalyzed Dimerization of *trans* Anethole: Detection of the Distonic Tetramethylene Radical Cation Intermediate by Extractive Electrospray Ionization Mass Spectrometry. J. Am. Chem. Soc. 130, 17208–17209 (2008). https://doi.org/10.1021/ja806791c
- 30. Bain, R.M., Pulliam, C.J., Cooks, R.G.: Accelerated Hantzsch electrospray synthesis with temporal control of reaction intermediates. Chem. Sci. 6, 397–401 (2015). https://doi.org/10.1039/C4SC02436B
- 31. Konermann, L., Rosell, F.I., Mauk, A.G., Douglas, D.J.: Acid-Induced Denaturation of Myoglobin Studied by Time-Resolved Electrospray Ionization Mass Spectrometry †. Biochemistry. 36, 6448–6454 (1997). https://doi.org/10.1021/bi970353j
- 32. Kharlamova, A., Prentice, B.M., Huang, T.-Y., McLuckey, S.A.: Electrospray Droplet Exposure to Gaseous Acids for the Manipulation of Protein Charge State Distributions. Anal. Chem. 82, 7422–7429 (2010). https://doi.org/10.1021/ac101578q
- 33. Simmons, D.A., Konermann, L.: Characterization of Transient Protein Folding Intermediates during Myoglobin Reconstitution by Time-Resolved Electrospray Mass Spectrometry with On-Line Isotopic Pulse Labeling †. Biochemistry. 41, 1906–1914 (2002). https://doi.org/10.1021/bi011697j
- 34. Badu-Tawiah, A.K., Campbell, D.I., Cooks, R.G.: Accelerated C–N Bond Formation in Dropcast Thin Films on Ambient Surfaces. J. Am. Soc. Mass Spectrom. 23, 1461–1468 (2012). https://doi.org/10.1007/s13361-012-0394-y
- 35. Eliezer, D., Chiba, K., Tsuruta, H., Doniach, S., Hodgson, K.O., Kihara, H.: Evidence of an associative intermediate on the myoglobin refolding pathway. Biophys. J. 65, 912–917 (1993). https://doi.org/10.1016/S0006-3495(93)81124-X

- 36. Breuker, K., McLafferty, F.W.: Stepwise evolution of protein native structure with electrospray into the gas phase, 10-12 to 102 s. Proc. Natl. Acad. Sci. 105, 18145–18152 (2008). https://doi.org/10.1073/pnas.0807005105
- 37. Feng, R., Konishi, Y.: Stepwise refolding of Acid-denatured myoglobin: Evidence from electrospray mass spectrometry. J. Am. Soc. Mass Spectrom. 4, 638–645 (1993). https://doi.org/10.1016/1044-0305(93)85028-V
- 38. Venter, A., Sojka, P.E., Cooks, R.G.: Droplet Dynamics and Ionization Mechanisms in Desorption Electrospray Ionization Mass Spectrometry. Anal. Chem. 78, 8549–8555 (2006). https://doi.org/10.1021/ac0615807
- 39. Yin, S., Loo, J.A.: Top-down mass spectrometry of supercharged native protein–ligand complexes. Int. J. Mass Spectrom. 300, 118–122 (2011). https://doi.org/10.1016/j.ijms.2010.06.032
- Badu-Tawiah, A.K., Campbell, D.I., Cooks, R.G.: Reactions of Microsolvated Organic Compounds at Ambient Surfaces: Droplet Velocity, Charge State, and Solvent Effects. J. Am. Soc. Mass Spectrom. 23, 1077–1084 (2012). https://doi.org/10.1007/s13361-012-0365-3
- 41. Zhou, S., Prebyl, B.S., Cook, K.D.: Profiling pH Changes in the Electrospray Plume. Anal. Chem. 74, 4885–4888 (2002). https://doi.org/10.1021/ac025960d
- 42. Radionova, A., Greenwood, D. R., Willmott, G. R., Derrick, P. J.: Dual Nano-Electrospray and Mixing in the Taylor Cone. *Mass Spectrom. Lett.*, 2016, **7**, 21–25

Graphical Abstract



Droplet pH: real-time N₂ pressure effect